Sensors & Actuators: A. Physical 371 (2024) 115255

Contents lists available at ScienceDirect

Sensors and Actuators: A. Physical

journal homepage: www.journals.elsevier.com/sensors-and-actuators-a-physical

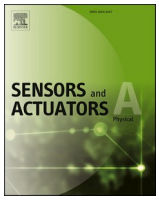

Estimation of the total current harmonic distortion using an ELF magnetometer

Francisco Portillo, Alfredo Alcayde, Rosa M. García, Nuria Novas, José Antonio Gázquez *, Manuel Fernández-Ros

Department of Engineering, University of Almeria, ceiA3, Almeria 04120, Spain

ARTICLE INFO

Keywords:
Harmonics
THD
Electrical power quality
Magnetometer
FFT

ABSTRACT

The conventional operation of the grid and electrical devices can be disturbed by harmonics, so standards impose strict limits on harmonic current. The entire grid is essential for today's society, but electromagnetic fields are radiated at their fundamental frequency and harmonics. This paper investigates a methodology to estimate the total current harmonic distortion of the grid by analyzing the magnetic flux density obtained from an extremely low-frequency magnetometer in the 0–2.2 kHz range. A Fast Fourier transform algorithm was applied to determine the magnetic flux density in the frequency domain. By evaluating the ratio of the fundamental component of the magnetic flux density to the harmonics, its total harmonic distortion rate could be deduced. Finally, the data were compared with measurements obtained by two power quality analyzers.

1. Introduction

With over a century of development, the electrical system has become one of the most widely implemented entities in the world, comprising various components necessary to bring electrical energy to any point where it is required. This system transports electrical power from generation plants to domestic, commercial, and industrial users, forming a vast network across countries [1]. In 2021, the electricity distribution network in Spain was extended to 44,769 km [2], and it was estimated to have 360,000 km of overhead power transmission networks [3]. Growing electrical power demand is critical to economic progress [4]. However, the ever-increasing problem is that electrical systems also radiate electromagnetic fields (EMFs) in their fundamental frequency and harmonics, collectively known as power line harmonic radiations (PLHRs) [5].

PLHRs are considered a source of artificial electromagnetic pollution [6] and are recognized as a significant problem related to electromagnetic compatibility [7]. They are generated in industrialized areas by the EMF radiating from ground power systems' transmission lines. The fundamental frequency (50/60 Hz) can be detected anywhere on Earth, reach near space, and even be observed by satellites [8]. PLHRs were first identified in 1975, and later, statistical analysis showed that the highest levels of PLHRs were observed around local noon, corresponding to periods of the most significant energy consumption [9]. Subsequently, data presented for Sundays indicated a decrease compared to other days of the week, interpreted as an influence of the energy consumption pattern [10].

Observations of PLHRs from the DEMETER satellite separated by 50/100 Hz were presented in [11]. They also found lines separated by 16.66 Hz, interpreted as an influence of the railway electrification system (some central and northern European countries follow the standard 15 kV voltage and 16 2/3 Hz frequency). Other authors also analyzed data from DEMETER and PLHR with a frequency gap of 50/100 Hz or 60/120 Hz, with the arrangement of the events perfectly matching the fundamental frequency of the power system of the generating regions [12].

The environmental problems caused by PLHRs have become an issue of increasing concern since they not only affect power quality (PQ), disrupt the ordinary service of the electrical grid and telecommunication systems, but also pollute the magnetosphere and

ionosphere [5]. Harmonic pollution is the primary PQ issue [13], and the main source of these harmonics is associated with nonlinear loads produced by switching devices [14]. Since the 1960 s, these have been used in industries where it is necessary to control the energy released in high active loads [15]. [16] estimated that nonlinear loads accounted for only 1.5% of total grid loads in 1987. However, the increasing complexity of the grid and the growth of power electronics have been the driving force behind the development of nonlinear loads in

* Corresponding author.
E-mail address: jgazquez@ual.es (J.A. Gázquez).

https://doi.org/10.1016/j.sna.2024.115255
Received 31 December 2023; Received in revised form 20 February 2024; Accepted 3 March 2024
Available online 7 March 2024

domestic, commercial, and industrial environments [17]. As a result, the number of nonlinear loads has increased exponentially in recent decades, estimated to reach 85% in 2012 [18].

Regarding PQ, EN 50160: 2010 'Voltage Characteristics of Electricity Supplied by Public Distribution Networks' [19] specifies the main characteristics of the voltage signal (frequency, amplitude, waveform, and symmetry) and the limits it is expected to maintain. However, unlike these PQ factors, which depend on the energy supplier, harmonic currents are disturbances that originate in the installations and are injected into the distribution system [20]. Therefore, disturbances in the power system are caused by power distribution companies and end users [21] and must be restricted. In this context, the standard IEC 61000–3–2:2018 'Electromagnetic Compatibility (EMC) - Part 3–2: Limits' [22] and IEC 61000–3–12: 2011 'Electromagnetic Compatibility (EMC) - Parts 3–12: Limits' [23] specify the limit of harmonic current that the equipment can inject into the network.

Whereas a combination of linear and nonlinear loads is fed from a perfectly sinusoidal supply, current pulses appear in the total supply current with a frequency that is a multiple of the fundamental frequency. Even-order harmonics (the 2nd, 4th, 6th, 8th, etc.) are generally not critical due to signal symmetry, and their magnitudes in low-voltage networks are assumed to be small [24]. Single-phase nonlinear loads, such as computers, electronic ballasts, and household appliances, among others, generate odd harmonics (the 3rd, 5th, 7th, 9th, etc.), being the 3rd and its odd multiples (the 9th, 15th, etc.), called 'triplens,' the most problematic. Nonlinear three-phase loads, such as inverters, three-phase rectifiers, converters, etc., produce the 5th and 7th harmonics and a minor proportion of the 11th and 13th [25]. In general, harmonic currents and the resulting harmonic voltages are the source of PQ problems and affect the efficiency of power grid users [26].

The detrimental effects of harmonics are increasingly significant in power systems [27] and can be summarized as follows.

- Efficiency losses in electrical installation and equipment;
- Functioning problems in electronic regulation devices, both power and control;
- Overheating electrical equipment (motors, transformers, generators, etc.) due to additional copper and iron losses;
- Reduce useful life, insulation degradation, increased energy losses, etc.;
- Malfunction of electronic protection and measurement devices;
- Untimely tripping of differential switches;
- Interference in telephone and data systems;
- Decrease in the power factor, aging, and even destruction of capacitor banks due to resonance and amplification phenomena;

In summary, nonlinear loads cause distortions that worsen PQ, making PQ monitoring essential for improving the performance of end-user loads and power system equipment [28]. This article explores a procedure to estimate the total harmonic distortion of the current signal (THD_C) of the grid by analyzing the magnetic flux density (B) obtained from an extremely low frequency (ELF) magnetometer.

The magnetic field is generated whenever electricity flows through a conductor, and its strength depends on the current on the wire [29]. Therefore, this magnetic field contains distortions because its source is the current signal with harmonic components. As the Biot-Savart law states, the magnitude of B in the magnetometer is inversely proportional to the cube of the distance [30] between the measurement point in the normal plane and the field source, so sources closer to the magnetometer have a more significant impact. In this way, it has been possible to compare the THD_C of the nearby grid by evaluating the ratio of the fundamental component of B to its harmonics, that is, the total harmonic distortion of B (THD_B).

The conventional approach for THD_C assessment, as guided by standards such as [22] and [23], typically involves the evaluation of harmonics generated by individual equipment connected to the low-voltage network. However, this method often necessitates physical connections to the network and may only be feasible for some area monitoring. In some scenarios where traditional PQ analyzers cannot be installed due to logistical or financial restrictions, an approach without physical connections could be helpful.

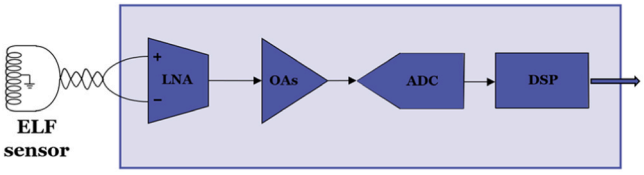

Fig. 1. Signal acquisition and preprocessing.

In this way, our system has been designed not to measure accurately the THD_C of specific equipment but to monitor overall THD_C across a wider area without requiring direct physical connections to the power network. However, one significant limitation is its inability to isolate THD_C measurements for individual phases. Our system has these limitations since the method provides a general assessment of the THD_C in a given area, capturing the aggregate effects rather than conducting a phase-specific analysis. This constraint, while notable, does not diminish the system's utility as a supplementary tool for PQ assessment, especially in large-scale and inaccessible areas.

2. Materials and methods

In this chapter, we report the materials and methods employed in this study. Data used for the calculations were collected in May 2021 and processed using the MatLab® R2021.a software package (MathWorks, Inc., MA, USA).

2.1. ELF magnetometer

Data sets come from the project UAL18-TIC-A025-A 'Monitored Electromagnetic Field Generated by Electrical Grids'. This project was initially created at the University of Almeria (UAL), Spain, to monitor the magnetic field generated by power lines and equipment in the 0–2.2 kHz range in real time. The magnetometer used for this project was located in a lab managed by the TIC019 Research Group on the UAL campus. The laboratory is situated in the 'Information and Communication Technology Research Center' (CITIC, in its Spanish acronym), which serves as a workspace for researchers and professors. Additionally, the building houses the Data Processing Center (DPC) and hosts the UAL headquarters of the central IT services. For this reason, the average power of this building (around 100 kW) is higher than that of the other buildings on campus.

The magnetometer encompasses a magnetic sensor (MS), an analog conditioning stage (ACS), an analog-to-digital converter (ADC), and a digital signal processor (DSP) (see Fig. 1), which undertakes initial data processing tasks. This setup was previously employed in earlier work by the authors [31].

The MS uses a coreless coil centered to the ground to create two equal windings with 12,000 turns of 0.25 mm diameter enameled copper wire. This setup is designed to measure vector B perpendicular to the sensor's area. The average diameter of the coil is 32 cm, and the winding width is 4.5 cm. The inductance of the sensor is 68.5 H, and the self-resonance frequency is 990 Hz. The maximum sensitivity of the sensor plus the amplification stage is 2.93 mV/pT at 632 Hz, while at 50 Hz the value is 57 μV/pT. Information on the geometry, structure, materials, amplification stage, and preprocessing stage of similar sensors can be found in [32].

The creation of a coil with a high number of turns is significant due to the notable size of the coil, the type of wire used, and its specific arrangement. Increasing the number of turns in the coil enhances its

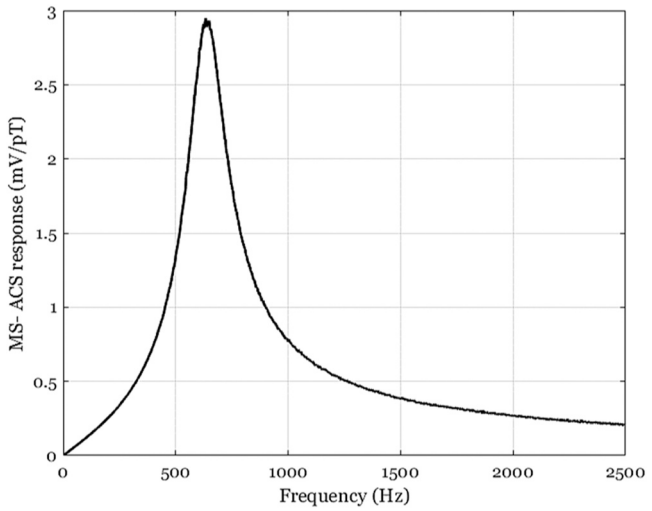

Fig. 2. MS and ACS response required for calibration.

sensitivity to changes in B, and the signal-to-noise ratio is improved, which facilitates the detection and analysis of weak magnetic fields. The MS was explicitly designed to measure ELF and weak magnetic fields. Its features make it especially useful for this purpose, although the configuration employed is restricted to measuring only the vertical component of the magnetic field. This limitation originates from its initial setup in the R&D project UAL18-TIC-A025-A, in which the equipment was configured with a single sensor aligned along the Z-axis. Based on empirical observations, the MS was aligned with the axis exhibiting the strongest magnetic field.

The ACS comprises three distinct amplification stages: an initial Low-Noise Amplifier (LNA) followed by two stages utilizing operational amplifiers, with respective gain factors of 100, 2, and 1. The ACS exhibits a frequency bandwidth of 2219.5 Hz. The 24-bit unit ADC performs oversampling of the amplified MS signal at a frequency (F_S') of 48,828 samples per second. Subsequent data preprocessing in the DSP involves signal decimation to achieve a final sampling rate (F_S) of 4439 SPS, with the data recorded at this FS constituting the system's raw output.

An error analysis was conducted to evaluate the system's accuracy. Specifications provided by the manufacturers of the INA110SG (LNA), LM833, and ADS1274 components informed the identification of primary error sources. The system exhibits a typical precision range of ±0.63% and, though less likely, can reach a maximum error margin of ±4.9%. It is pertinent to note that these accuracy figures are calculated before applying any corrective measures.

The system's calibration necessitates the MS and the ACS responses, represented in Fig. 2 and determined using the Agilent Model E5061B Vector Network Analyzer.

2.2. Harmonic measurement

The magnetometer output signal corresponds to *B*. Once confirmed that all signals captured and measured by the system are magnetic (noise floor of the ACS approximately 10^{-4} nT), *B* is transformed from time to frequency domain using the fast Fourier transform (FFT) algorithm.

The total harmonic distortion factor (THD_Y) is employed to express the non-sinusoidal property of the waveform of the signal Y. THD_Y can collectively describe the severity of harmonic disturbances according to Eq. (1) [13]:

$$THD_Y = \frac{\sqrt{\sum_{h=2}^{hmax} Y_h^2}}{Y_1} 100\% \quad (1)$$

where Y_h is the root mean square (RMS) of the individual harmonic of order *h*, Y_1 corresponds to the RMS value of the fundamental component, and h_{max} is the maximum order. This article has considered a maximum order of 40 (corresponding to 2 kHz).

The accuracy of FFT analysis requires a stationary signal, but signals can fluctuate and spread the energy of the harmonic components to the contiguous spectral intervals [33]. For this reason, IEC 61000–4–7:2002 'Electromagnetic Compatibility (EMC) - Parts 4–7: Testing and Measurement Techniques: General Guide on Harmonic and Interharmonics Measurements and Instrumentation, for Power Supply Systems and Equipment Connected Thereto' [34] introduces the notion of spectral line grouping.

2.3. Grouping

The output of the FFT algorithm is first grouped to form the square sum of the intermediate spectral bars existing between two adjacent harmonics to improve accuracy, as shown in Fig. 3. Each batch is called a 'group' and comprises frequencies of ± 25 Hz around each harmonic. A similar evaluation could be performed if the harmonics and interharmonics were evaluated separately, but the frequencies would be ±

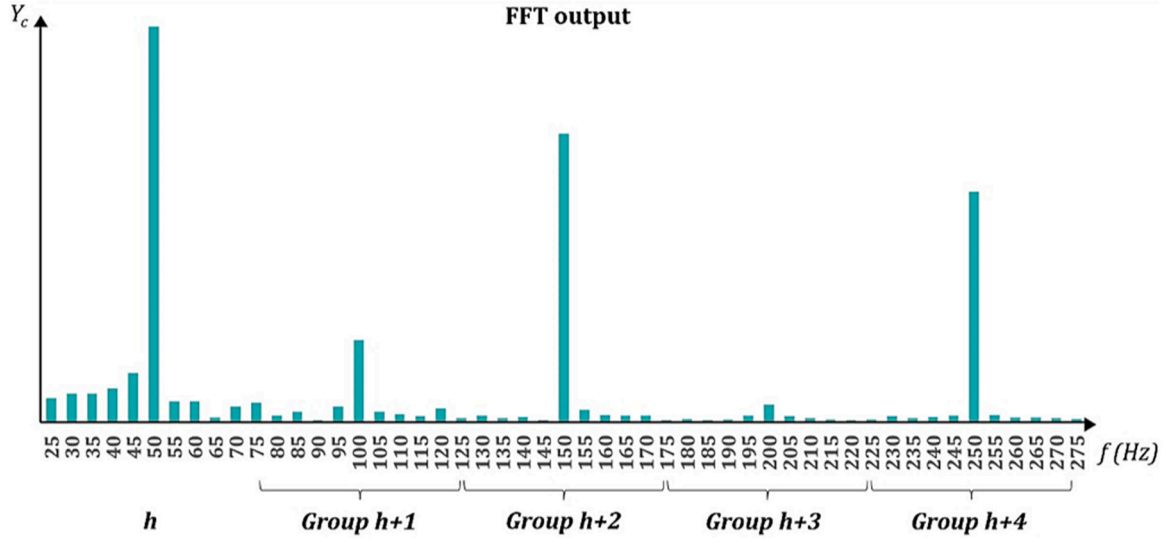

Fig. 3. Representation of harmonic groups for 50 Hz grids.

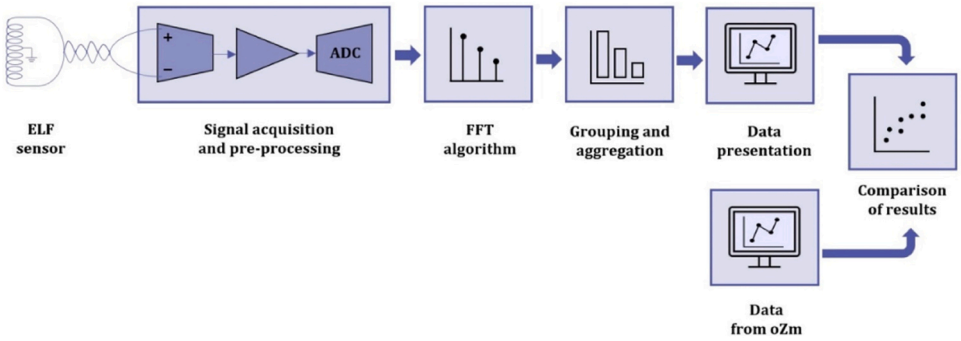

Fig. 4. Block diagram of the system used in this paper.

Fig. 5. (a) Buildings and outdoor lighting near the ELF magnetometer, (b) public streetlight, (c) led streetlights, and (d) HPS lamp.

5 Hz around each harmonic and would be called a 'subgroup' [33].

For 50 Hz grids and considering a spectral resolution of 5 Hz, the resulting harmonic group is obtained according to Eq. (2) of the standard [34]:

$$Y^2_{g,h} = \frac{Y^2_{C,k-5}}{2} + \sum_{i=-4}^{4} Y^2_{C,k+i} + \frac{Y^2_{C,k+5}}{2} \tag{2}$$

where $Y_{g,h}$ is the RMS value of the harmonic group of order h, and $Y_{C,\,k+i}$ is the RMS value of a spectral bar of the FFT.

Once the groupings have been made, Eq. (2) becomes Eq. (3):

$$THDG_Y = \frac{\sqrt{\sum_{h=2}^{hmax} Y^2_{g,h}}}{Y_{g,1}} 100\% \tag{3}$$

where now $Y_{g,h}$ is the RMS of the individual harmonic group of order h, and $Y_{g,1}$ is the RMS of the group corresponding to the fundamental component.

IEC 61000–4–30: 2015 'Electromagnetic Compatibility (EMC)-Part 4–30: Testing and Measurement Techniques-Power Quality Measurement Methods' [35] defines measurement methods and interprets the results of the PQ parameters. The different techniques are related for each parameter type to obtain reliable and repeatable results, so other methods are implementation independent. This standard includes various categories of aggregation algorithms for PQ factors. This article used the 10-minute aggregation algorithm to obtain a $THDG_Y$ value every 10 minutes.

2.4. Comparison of results

In our case, the output is B, which comes from the nearby grid. The THD_B was calculated by evaluating the ratio between the fundamental component of B and its harmonics. Our results were contrasted with data obtained from two commercial PQ analyzers to compare these values with the TDH_C of the grid. For this purpose, the Openzmeter (oZm) analyzer [36] was selected, which shows the THD_C value every 15 minutes. This analyzer has been used successfully in previous work by the authors [31] [37], as the device includes open hardware and free software. The first analyzer was placed on the electrical switch of the main electrical box, and the second was installed on the outside lighting power line. Fig. 4 shows a block diagram of the system used in this article.

Fig. 5(a) shows a plan of the UAL campus with the magnetometer location inside the CITIC and the outside lighting around the building. A programmable astronomic twilight switch activates the campus streetlights (Fig. 5(b)), automatically changing the on/off period depending on the day of the year. Furthermore, the decorative lighting (Fig. 5(c)) is turned off between 00:00 am and 6:00 am. The primary public streetlights on the UAL campus still use high-pressure sodium lamps (HPS) (Fig. 5(d)). These lamps do not have a high unit power. However, they are an essential source of harmonics, as many are used simultaneously for an extended period.

3. Result and discussion

All timescales in this document were plotted in Spain's local time, not in universal coordinated time (UTC). The graphs help better understand the results, influenced by local habits, such as peak hours and night lighting.

Once the ELF magnetometer signal has been processed and the data are grouped and aggregated, the output corresponds to the RMS value of B in nT generated by the electrical lines and devices around the sensor location. Fig. 6(a) illustrates the value of B over a 10-minute interval for each frequency up to 2 kHz. The y-axis has been plotted on a logarithmic scale to appreciate all spectral components, and the data correspond precisely to the interval between 07:00 am and 07:10 am on 7 May 2021. Fig. 6(b) shows the detail up to the harmonic 15th on a linear scale. Following the same procedure, B was calculated every 10 minutes throughout May.

The expression of harmonics as a percentage of the fundamental can

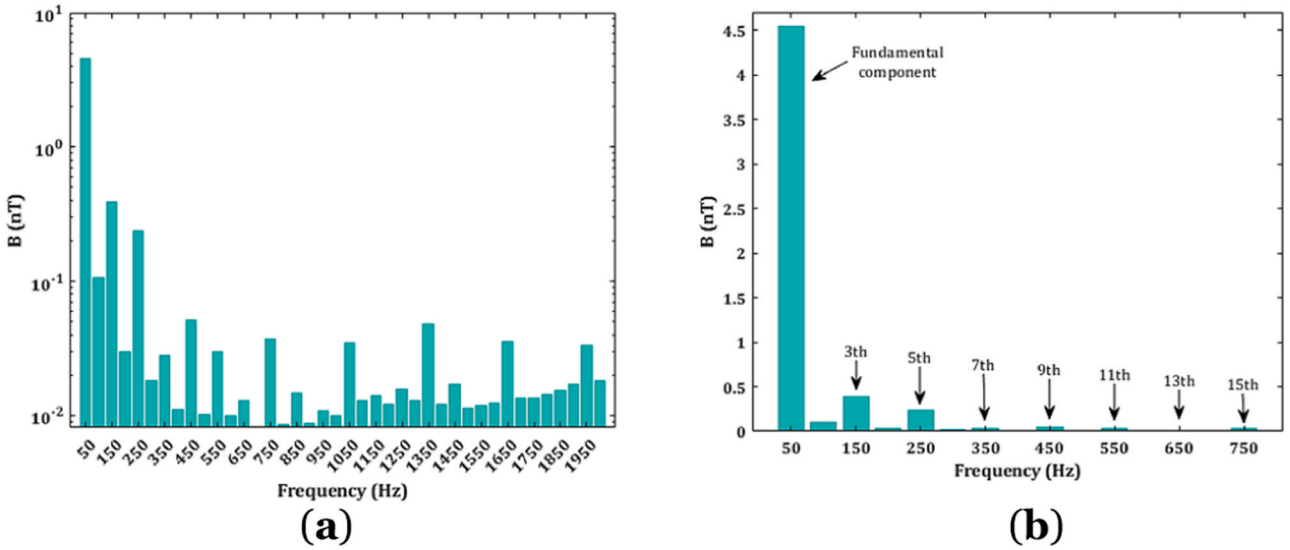

Fig. 6. *B* in the frequency domain. (a) Up to 2 kHz and (b) up to harmonic 15th.

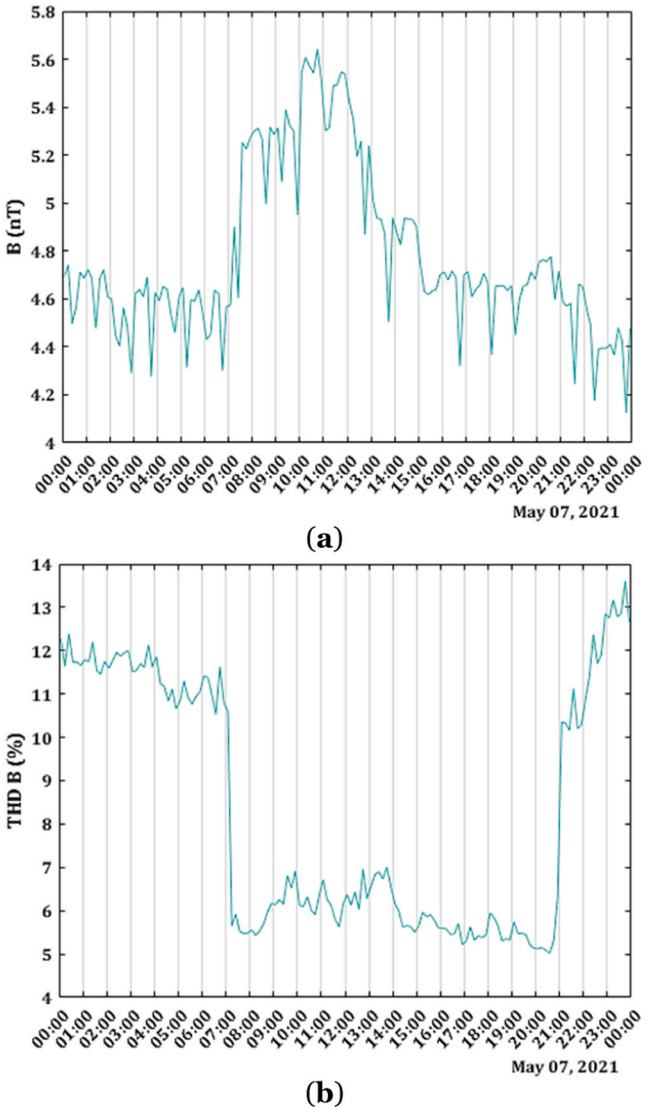

Fig. 7. Data on 7 May 2021. (a) *B* and (b) THD_B.

help to understand relative harmonic levels [38]. However, this work grouped the fundamental component and harmonics to order 40 in an RMS value. Its evolution on 7 May 2021 is shown in Fig. 7(a). Furthermore, the THD_B is calculated according to Eq. (3), obtaining the values shown in Fig. 7(b).

In Fig. 8, a comparison is shown between *B* and the electricity consumption of the building where the sensor was installed. *B* captured by the ELF sensor on 7 May 2021 is shown on the left axis, and the electricity consumption of the CITIC is shown on the right axis. The figure demonstrates that the electrical consumption of the building has an impact on *B* captured by the sensor. As noted above, *B* is inversely proportional to the cube of the distance between the measurement point and the field source. The primary influence on the sensor is the power consumption of the building where it is located. However, other buildings and power lines on campus also have a lesser impact.

According to [39], the electricity demand in a grid is represented by its daily load curve, which generally has a minimum at dawn and a peak at noon or late afternoon. This curve depends on the time of year, usage (industry, residential, offices, etc.), climatology, and population habits. In our case, the evolution of *B* throughout the day follows a typical consumption curve of an office building. It increases at 7 am, peaks at midday, and decreases from 3 pm onward. To assess the impact of weekends and holidays, Fig. 9(a) compares 8 May 2021 (Saturday), and Fig. 9(b) corresponds to 9 May 2021 (Sunday). The daily curve is flatter on both days analyzed.

A second comparison was conducted between the obtained THD_B and the THD_C provided by the PQ analyzers. A noteworthy event is a sudden change in the THD_B at approximately 7 am and 9 pm. Close analysis reveals that the abrupt changes occur at dawn and dusk. Fig. 10 (a) displays the THD_B for Saturday, 1 May 2021, with dawn occurring at 7:16 am and dusk at 8:57 pm. Fig. 10(b) shows the THD_B for Monday, 31 May 2021, with dawn at 6:53 am and dusk at 9:21 pm. The first and last days of May were selected to highlight how dawn and dusk depend on the time of year and confirm that sudden variations occur at these moments.

According to Fig. 10, the outside lighting surrounding the CITIC affects the THD_B at night. Nonlinear single-phase loads, such as HPS lamps of the outside lighting, produce a significant content of current harmonics, with the 3rd being the highest. Fig. 11 compares the THD_B captured by the ELF sensor and the THD_C provided by the PQ analyzers. As mentioned previously, the analyzers were installed on the main electrical switches of the lines, which are three-phase; thus, the THD_C result is obtained for each of the three phases. Fig. 12 presents the same

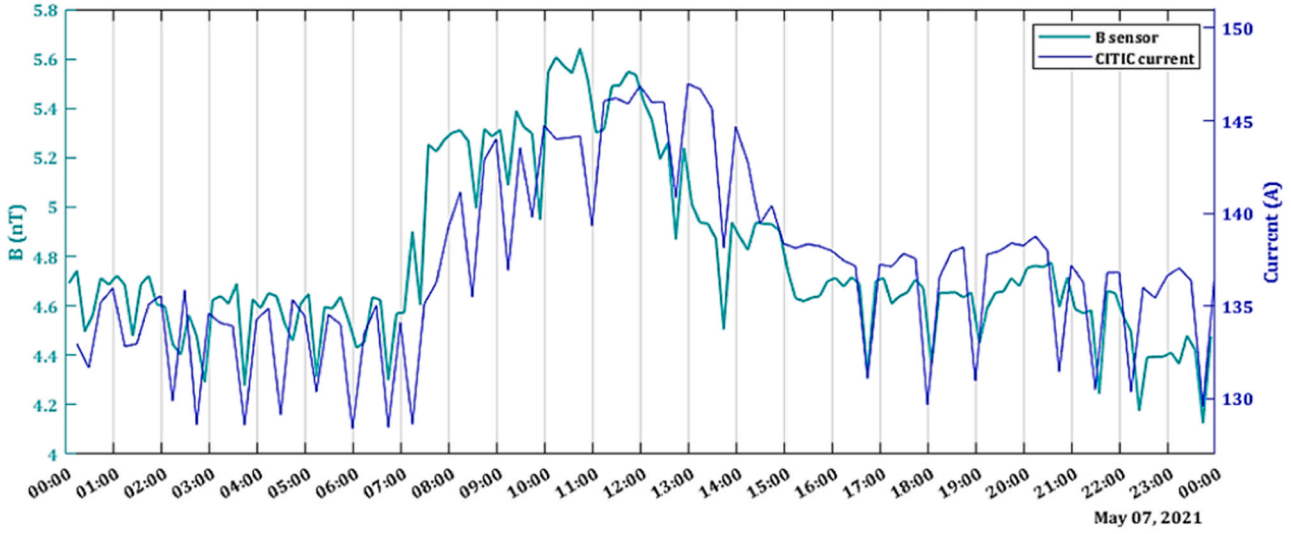

Fig. 8. Comparison between *B* and electricity consumption on 7 May 2021.

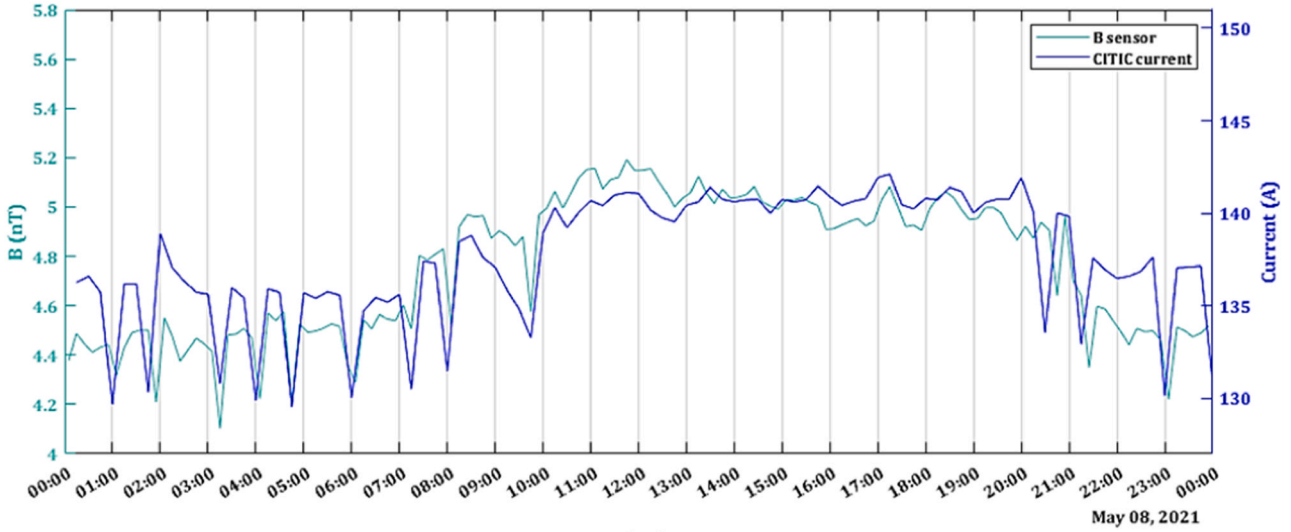

(a)

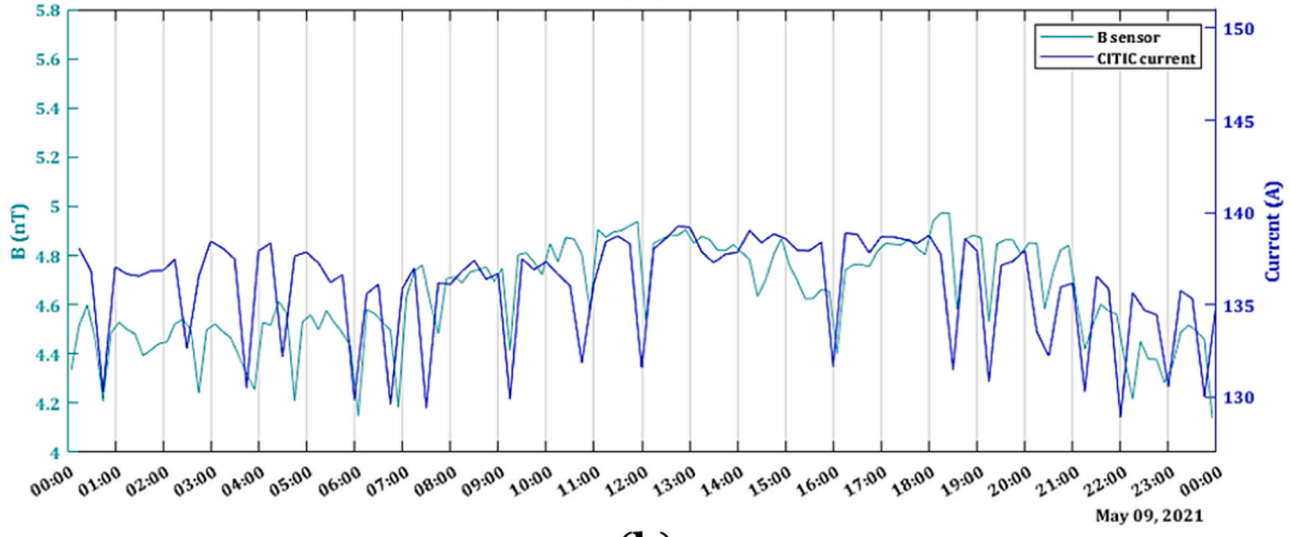

(b)

Fig. 9. Comparison between *B* and electricity consumption (a) 8 May 2021, Saturday, and (b) 9 May 2021, Sunday.

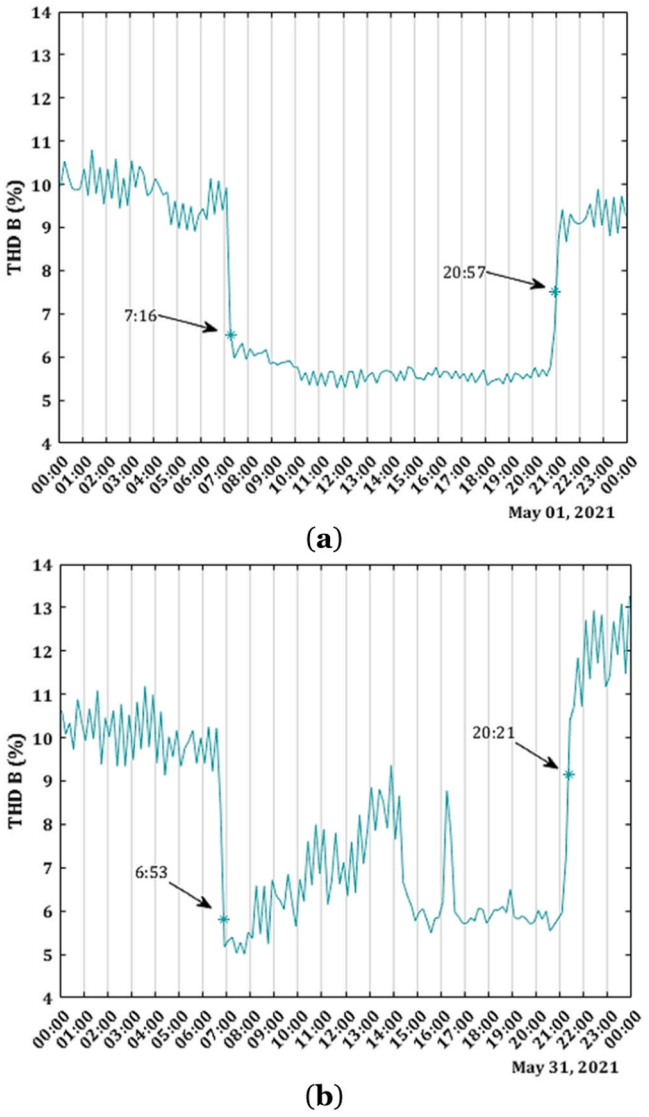

Fig. 10. THD_B. (a) 1 May 2021 and (b) 31 May 2021.

comparison but with the resulting THD_C of both PQ analyzers.

Fig. 12 shows that the THD_B matches the THD_C during daylight. However, the values diverge during the night period. In a closer analysis, Fig. 13 presents a monthly breakdown of THD during the day. Throughout May, the mean THD_B captured by the ELF sensor during daylight matches the THD_C values. The maximum difference occurs on 18 May, with a difference between THD_B and the THD_C L_3 of 1.10%.

On the other hand, when the night period begins, and the outside lighting is turned on, the THD_B increases and remains higher than the THD_C obtained by the PQ analyzers. Fig. 14 presents a monthly analysis of THD during the night period. Throughout May, the mean THD_B obtained in the ELF sensor in the night period was higher than the THD_C measured by the analyzers. The maximum difference occurs on May 18, with a value of 3.54% between THD_B and THD_C L_3. This indicates that the electrical line and streetlights of the outside lighting are closer to the ELF sensor than the DPC (see Fig. 5(a)), and therefore, the data obtained by the sensor are more influenced by this line. According to the Biot-Savart law, the most considerable influence

on the ELF sensor is due to the electrical consumption of the building where the sensor is installed and the outside lighting surrounding it. However, it is also influenced to a lesser extent by the rest of the buildings and power lines on the UAL campus. The evolution of B throughout the day matches the daily consumption curve of a building, and even the effects of weekends and holidays have been checked. During the daylight period, the THD_B follows the THD_C of the CITIC. In contrast, the main characteristic of the night period is that the level of the 3rd harmonic increases because of the type of lamp used in the outside lighting, which causes the growth of the THD_B. The ELF magnetometer receives more significant intensity harmonics that are best propagated, those with the highest frequency.

Electric power is essential to modern life; therefore, EMFs are ubiquitous in our environment. This topic is of great interest to society due to the continuous exposure of the general population [40]. EMF research covers various areas, such as medicine, engineering, astrophysics, etc. Although most publications in the medical field focus on the harmful effects that low-frequency radiation could have on human health, a monograph by the World Health Organization [41] concluded that there are no substantial health problems related to ELF radiation at levels typical of domestic environments.

PQ is a widely discussed topic in electrical engineering. Recently, a wide range of sensors have been developed to monitor power grids [42]; yet, to our knowledge, only a few articles have been published linking EMF research and quality monitoring of the grid. In a previous paper by

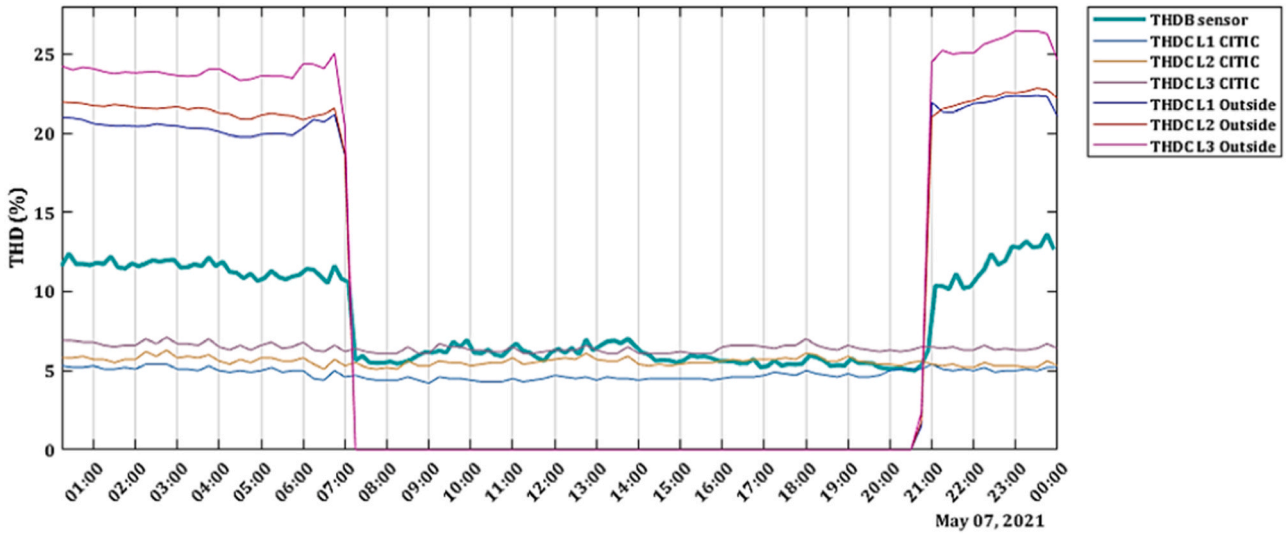

Fig. 11. Comparison between the THD_B and the THD_C of the CITIC and the outside lighting for 7 May 2021.

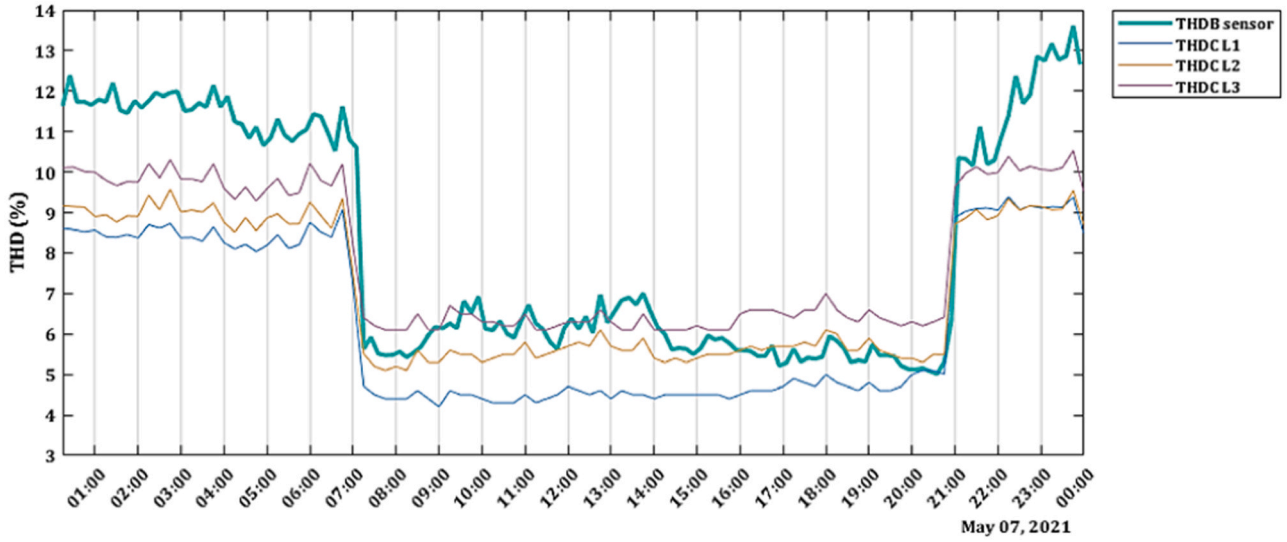

Fig. 12. Comparison between the THD_B and the resulting THD_C for 7 May 2021.

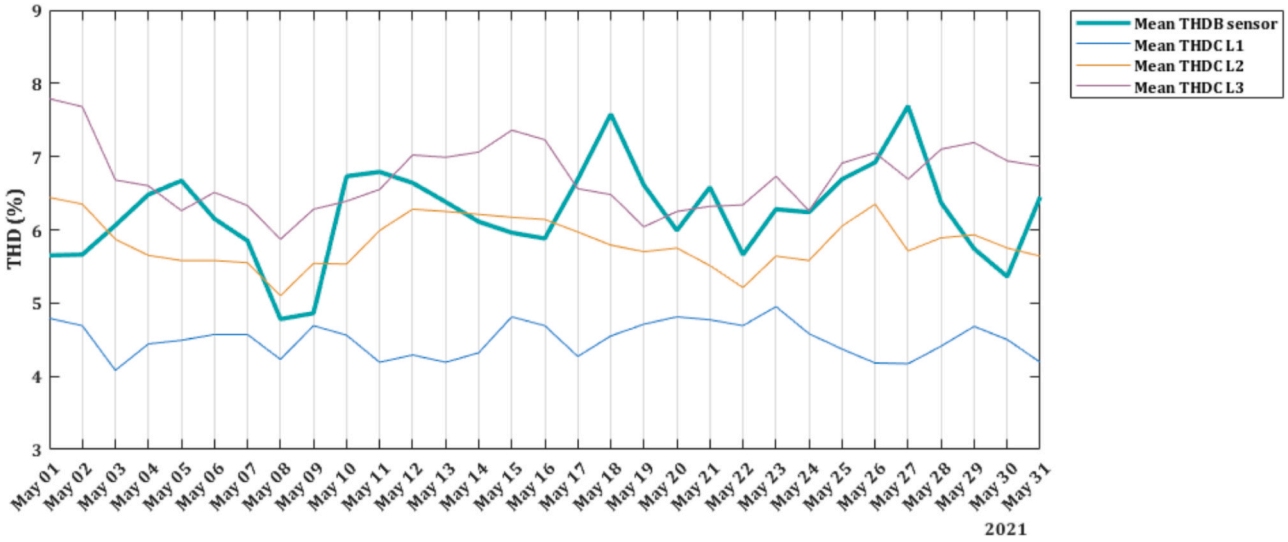

Fig. 13. Mean *THD* during the daylight period of May 2021.

the authors [31], a procedure was developed to calculate the grid frequency from data obtained from an ELF magnetometer. This paper focuses on the methodology to estimate the THD_C of an area non-invasively by analyzing the data from an ELF magnetometer. In [43], the harmonics are calculated near an overhead power line, but work has yet to be found in urban environments with different sources.

4. Conclusions

The EMF produced by electrical devices and installations has been monitored by an ELF magnetometer developed by our Research Group. A full year of data has been collected, specifically from September 2020 to September 2021. With this processed information, B and its THD_B were found for May 2021.

After analyzing the results, the measurement of the THD_C of the area surrounding the ELF magnetometer was performed indirectly and non-invasively. The validation procedure with two commercial devices contrasts the results obtained.

Unlike other factors in PQ, such as voltage, amplitude, frequency, or symmetry, which depend on the energy supplier, harmonic currents are disturbances that originate in the facilities themselves and are injected into the distribution system. Therefore, these disturbances in the electrical power system are due to electrical distributors, end users, engineers, and manufacturers. Consequently, a more substantial

number of measurements of PQ parameters are necessary as electrical consumption increases. Generally, THD_C measurement is performed using techniques that require a connection point. In our case, the data input source is the EMF radiated by devices and electrical lines; therefore, it is possible to measure non-invasively without a connection point. This way, we can monitor an area using portable equipment without physical contact. This approach does not interfere with the users of the electrical grid. Our research demonstrates the feasibility and effectiveness of using an ELF magnetometer system for broad-area THD_C monitoring in electrical networks. This method offers a practical approach to power quality monitoring, supplementing traditional methods and extending the scope of THD_C assessment to areas where conventional PQ analyzers are not viable. This capability can facilitate preventive maintenance and guide further investigation using more traditional methods.

Redesigning the system into a more compact and portable device

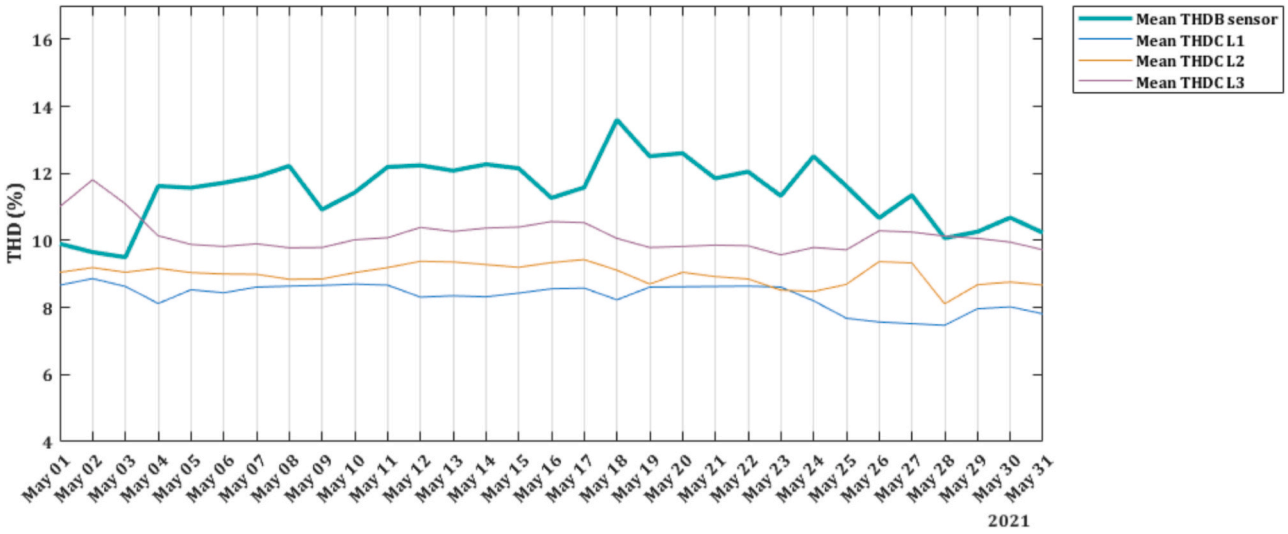

Fig. 14. Mean *THD* during the night period of May 2021.

could lead to tangible progress. For example, inserting a high-permeability ferrite core into the coil or changing to an ultrathin wire would reduce the size of the sensor. Additionally, the bandwidth could be extended to 9 kHz since some PQ standards reach this frequency.

Other improvements should aim to monitor more buildings on the UAL campus to determine the range of influence of our ELF sensor. This way, advances would be made in the PQ field by monitoring the grid and improving the knowledge of low frequency EMFs.

CRediT authorship contribution statement

Rosa Garcia-Salvador: Writing – review & editing. **Nuria Novas-Castellano:** Writing – review & editing, Visualization. **Jose A. Gazquez:** Writing – review & editing, Supervision, Methodology, Conceptualization. **Manuel Fernandez-Ros:** Writing – review & editing, Software, Methodology, Conceptualization. **Francisco Portillo:** Writing – review & editing, Methodology, Conceptualization. **Alfredo Alcayde:** Writing – original draft, Supervision, Software.

Declaration of Competing Interest

The authors declare that they have no known competing financial interests or personal relationships that could have appeared to influence the work reported in this paper.

Data availability

Data will be made available on request.

Acknowledgments

Under Project UAL18-TIC-A025-A, University of Almeria, Ministry of Economy, Knowledge, Business and University, and the European Regional Development Fund (FEDER); Andalusian Regional Government through the Electronics, Communication, and Telemedicine Research Group of the University of Almeria, Spain; and in part by the European Union FEDER Program and CIAMBITAL Group.

References

[1] L. Matikainen, M. Lehtomäki, E. Ahokas, J. Hyyppä, M. Karjalainen, A. Jaakkola, A. Kukko, T. Heinonen, Remote sensing methods for power line corridor surveys, ISPRS J. Photogramm. Remote Sens. 119 (2016) 10–31, https://doi.org/10.1016/j.isprsjprs.2016.04.011.

[2] Red Eléctrica de España., El sistema eléctrico español 2021, (2022). ⟨https://www.ree.es/sites/default/files/publication/2022/03/downloadable/Avance_ISE_2021.pdf⟩ (accessed April 13, 2022).

[3] P. Gajšek, P. Ravazzani, J. Grellier, T. Samaras, J. Bakos, G. Thuróczy, Review of studies concerning electromagnetic field (EMF) exposure assessment in Europe: low frequency fields (50 Hz–100 kHz), Int J. Environ. Res Public Health 13 (2016) 875, https://doi.org/10.3390/ijerph13090875.

[4] N. Novas, R.M. Garcia, J.M. Camacho, A. Alcayde, Advances in solar energy towards efficient and sustainable energy, Sustainability 13 (2021) 6295, https://doi.org/10.3390/su13116295.

[5] J. Wu, J.-J. Fu, C. Zhang, Propagation characteristics of power line harmonic radiation in the ionosphere, Chin. Phys. B 23 (2014) 034102, https://doi.org/10.1088/1674-1056/23/3/034102.

[6] J. Wu, Q. Guo, X. Yan, C. Zhang, Theoretical analysis on affecting factors of power line harmonic radiation, IEEE Trans. Plasma Sci. 47 (2019) 770–775, https://doi.org/10.1109/TPS.2018.2865827.

[7] J. Wu, Q. Guo, C. Yue, L. Xie, C. Zhang, Special electromagnetic interference in the ionosphere directly correlated with power system, IEEE Trans. Electro Compat. 62 (2020) 947–954, https://doi.org/10.1109/TEMC.2019.2918280.

[8] S.M. Werner, C.J. Rodger, N.R. Thomson, Identifying power line harmonic radiation from an electrical network, Ann. Geophys. 23 (2005) 2107–2116, https://doi.org/10.5194/angeo-23-2107-2005.

[9] C.G. Park, R.A. Helliwell, Magnetospheric effects of power line radiation, Science 200 (1979) (1978) 727–730, https://doi.org/10.1126/science.200.4343.727.

[10] C.G. Park, T.R. Miller, Sunday decreases in magnetospheric VLF wave activity, J. Geophys. Res. 84 (1979) 943, https://doi.org/10.1029/JA084iA03p00943.

[11] M. Parrot, F. Němec, O. Santolík, J.J. Berthelier, ELF magnetospheric lines observed by DEMETER, Ann. Geophys. 23 (2005) 3301–3311, https://doi.org/10.5194/angeo-23-3301-2005.

[12] F. Němec, O. Santolík, M. Parrot, J.J. Berthelier, Power line harmonic radiation: a systematic study using DEMETER spacecraft, Adv. Space Res. 40 (2007) 398–403, https://doi.org/10.1016/j.asr.2007.01.074.

[13] Ł. Michalec, M. Jasiński, T. Sikorski, Z. Leonowicz, Ł. Jasiński, V. Suresh, Impact of harmonic currents of nonlinear loads on power quality of a low voltage network–review and case study, Energies (Basel) 14 (2021) 3665. https://doi.org/10.3390/en14123665.

[14] J. Arrillaga, B.C. Smith, N.R. Watson, A.R. Wood, John. Power System Harmonic Analysis, Wiley & Sons, Ltd,., West Sussex, England,, 1997, https://doi.org/10.1002/9781118878316.

[15] A.V. Kostrov, M.E. Gushchin, A.V. Strikovskii, Generation and radiation of high power line harmonics, Geomagn. Aeron. 57 (2017) 482–490, https://doi.org/10.1134/S0016793217030094.

[16] M. Mohammad, Y.A. Mohammad, A.S.A. Amir, 3D electromagnetic study of transformers flux line distribution and losses determination under harmonic distortion caused by electronic equipments, Sci. Res. Essays 6 (2011) 4414–4420, https://doi.org/10.5897/SRE11.901.

[17] B. Singh, A. Chandra, K. Al-Haddad, Power Quality Problems and Mitigation Techniques, John Wiley & Sons Ltd,, Chichester, United Kingdom, 2015, https://doi.org/10.1002/9781118922064.

[18] A. Priyadharshini, N. Devarajan, A.R. Uma Saranya, R. Anitt, Survey of harmonics in non linear loads, Int. J. Recent Technol. Eng. (IJRTE) (2012) 2277–3878.

[19] European Committee for Electrotechnical Standarization (CENELEC), EN 50160: 2010—Voltage characteristics of electricity supplied by public distribution networks, European Committee for Electrotechnical Standarization (CENELEC): Brussels, Belgium, 2010.

[20] M.J. Ghorbani, H. Mokhtari, Impact of Harmonics on Power Quality and Losses in Power Distribution Systems, Int. J. Electr. Comput. Eng. (IJECE) 5 (2015) 166, https://doi.org/10.11591/ijece.v5i1.pp166-174.
[21] A. Vinogradov, A. Vinogradova, V. Bolshev, Analysis of the quantity and causes of outages in LV/MV electrical grids, CSEE J. Power Energy Syst. 6 (2020), https://doi.org/10.17775/CSEEJPES.2019.01920.
[22] International Electrotechnical Commission (IEC), IEC 61000-3-2: 2018—Electromagnetic Compatibility (EMC)—Part 3-2: Limits—Limits for Harmonic Current Emissions (Equipment Input Current ≤ 16 A per Phase), International Electrotechnical Commission (IEC): Geneva, Switzerland, 2018.
[23] International Electrotechnical Commission (IEC), IEC 61000-3-12: 2011—Electromagnetic Compatibility (EMC)—Part 3-12: Limits—limits for harmonic current produced by equipment connected to public low-voltage systems with input current >16 A and ≤ 75 A per Phase, International Electrotechnical Commission (IEC): Geneva, Switzerland, 2011.
[24] J. Barros, M. De Apraiz, R.I. Diego, Characterization of even harmonics in power system networks. IEEE International Instrumentation and Measurement Technology Conference (I2MTC), IEEE,, 2020, pp. 1–6 (202010.1109/I2MTC43012.2020.9128756).
[25] P. Sivaraman, C. Sharmeela, Power quality and its characteristics. Power Quality in Modern Power Systems, Elsevier,, 2021, pp. 1–60, https://doi.org/10.1016/B978-0-12-823346-7.00001-3.
[26] I. Hunter, Power quality issues: a distribution company perspective, Power Eng. J. 15 (2001) 75–80, https://doi.org/10.1049/pe:20010203.
[27] T.L. Skvarenina, The Power electronics handbook, Choice Rev. Online 40 (2002) 40-0320–40–0320, https://doi.org/10.5860/CHOICE.40-0320.
[28] Jasiński Sikorski, Kostyła Kaczorowska, Leonowicz Rezmer, Szymańda Janik, Bejmert Rybiański, Jasińska, Influence of measurement aggregation algorithms on power quality assessment and correlation analysis in electrical power network with PV power plant, Energy 12 (2019) 3547, https://doi.org/10.3390/en12183547.
[29] Z. Ou, C. Lu, A. Yang, H. Zhou, Z. Cao, R. Zhu, H. Gao, Self-biased magnetoelectric current sensor based on SrFe 12 O 19 /FeCuNbSiB/PZT composite, Sens Actuators A Phys. 290 (2019), https://doi.org/10.1016/j.sna.2019.03.008.
[30] O.K. Likkason, Exploring and using the magnetic methods. Advanced Geoscience Remote Sensing, InTech,, 2014, https://doi.org/10.5772/57163.
[31] F. Portillo, A. Alcayde, R.M. García, N. Novas, J.A. Gázquez, M. Férnadez-Ros, Grid frequency measurement through a PLHR analysis obtained from an ELF magnetometer, Sensors 22 (2022) 2954, https://doi.org/10.3390/s22082954.
[32] J.A.Gazquez Parra, M.Fernandez Ros, N.Novas Castellano, R.M.Garcia Salvador, Techniques for Schumann resonance measurements: a comparison of four amplifiers with a noise floor estimate, IEEE Trans. Instrum. Meas. 64 (2015) 2759–2768, https://doi.org/10.1109/TIM.2015.2420376.
[33] M. Aiello, A. Cataliotti, S. Nuccio, A PC-based instrument for harmonics and interharmonics measurement in power supply systems, Measurement 35 (2004) 371–380, https://doi.org/10.1016/j.measurement.2004.03.005.
[34] International Electrotechnical Commission (IEC)., IEC 61000-4-7. EMC - Testing and measurement techniques – General guide on harmonics and interharmonics measurements and instrumentation, for power supply systems and equipment connected thereto, (2002).
[35] International Electrotechnical Commission (IEC)., IEC 61000-4-30: 2015—Electromagnetic Compatibility (EMC)—Part 4-30: Testing and Measurement Techniques—Power Quality Measurement Methods, International Electrotechnical Commission (IEC): Geneva, Switzerland, 2015.
[36] openZmeter, What is openZmeter? Smart metering and power quality analysis for the people, (2018). ⟨https://openzmeter.com/⟩ (accessed December 17, 2021).
[37] F.M. Montoya, F.G.; Baños, R.; Alcayde, A.; Arrabal-Campos, Efficient open-source power quality analyser and smart meter, 25th International Conference on Electricity Distribution CIRED 2019 (2019).
[38] T.M. Blooming, D.J. Carnovale, Application of IEEE STD 519-1992 Harmonic Limits. Proceedings of the Conference Record of 2006 Annual Pulp and Paper Industry Technical Conference, IEEE,, 2006, pp. 1–9, https://doi.org/10.1109/PAPCON.2006.1673767.
[39] F. Baena, F.J. Muñoz-Rodriguez, P. Gómez Vidal, G. Almonacid, A new approach to estimate from monitored demand data the limit of the coverage of electricity demand through photovoltaics in large electricity grids, Sensors 20 (2020) 4390, https://doi.org/10.3390/s20164390.
[40] G. Betta, D. Capriglione, G. Cerro, G. Miele, M.S. D'amata, Human Exposure to 4G LTE Systems: enhancing the reliability of EMF extrapolation techniques based on spectrum analyzer measurements, IEEE Trans. Instrum. Meas. 70 (2021), https://doi.org/10.1109/TIM.2021.3106683.
[41] E. Van Deventer, C. Ohkubo, R. Saunders, E. van Rongen, L. Kheifets, C. Portier, Environmental Health Criteria, Monograph 238: Extremely Low Frequency Fields, WHO,, 2007.
[42] F. Rodríguez, I. Sánchez-Guardamino, F. Martín, L. Fontán, Non-intrusive, self-supplying and wireless sensor for monitoring grounding cable in smart grids, Sens Actuators A Phys. 316 (2020) 112417, https://doi.org/10.1016/j.sna.2020.112417.
[43] A. Mujezinović, E. Turajlić, A. Alihodžić, M.M. Dedović, N. Dautbašić, Calculation of magnetic flux density harmonics in the vicinity of overhead lines, Electronics 11 (2022) 512, https://doi.org/10.3390/electronics11040512.

Francisco Portillo Rodríguez, Industrial Engineer from the University of Malaga, Spain. He received his Ph.D. in 2023 from the University of Almeria, Spain. He is a temporary lecturer in the Electronics Technology area, Department of Engineering, University of Almeria. His work focuses on electromagnetic signals radiated by electrical networks. He has 15 years of experience in the private sector, performing his role in some positions of industrial maintenance and automation of processes.

Alfredo Alcayde García received his M. in computer science engineering at the University of Almería, Spain. He received his Ph.D. in 2011 at the University of Almería. He is a member of the Engineering Department at the University of Almeria and has spent two years researching and teaching power systems, energy savings, and optimization. He has published over 75 articles in journals, conferences, and workshops and several publications in books and conference proceedings.

Rosa María García Salvador graduated in Physics from the University of Granada, Spain, in 2007; Materials Engineering from the University of Almeria, Spain, in 2013; and a Ph.D. from the University of Almeria in 2012. She is a Ph.D. professor at the University of Almeria in the Electronics Technology area. Part of the Research Group TIC019 "Electronics, communications, and Telemedicine," her work is focused on Schumann resonance, ELF waves, electromagnetic sensors, and PLHR events.

Nuria Novas Castellano received a Ph.D. in electronics in 2007 from the University of Almeria, Spain. She has been an Associate Professor with the Department of Engineering, University of Almería, since 1999. Her research interests include electronics systems and wireless sensorization.

Jose A. Gázquez Parra received a Ph.D. in telecommunications from the University of Malaga, Spain, in 2002. He was an Associate Professor at the University of Granada, Spain. From 1990–1992, he was Chief Engineer with Ingeniería y Control Remoto S.A., Granada. He is currently a Professor at the Department of Engineering, University of Almeria, since 1992. He is the leading researcher at the Researching Group: Electronic Communications and Telemedicine (TIC019) from the Andalusian Research Plan. His research interests include electronics theory, embedded system design, and electromagnetic sensing.

Manuel Fernández Ros graduated in telecommunications engineering from the University of Alcalá de Henares, Spain. He received his Ph.D. in 2015 from the University of Almería, Spain. He is an Associate Professor in the Department of Engineering, University of Almeria. His research interests include DSP systems, electronic design, and electromagnetic phenomena.